A Pure-Compact Scheme for the Streamfunction Formulation of Navier-Stokes Equations

Matania Ben-Artzi
Institute of Mathematics
The Hebrew University, Jerusalem 91904, Israel
email: mbartzi@math.huji.ac.il

Jean-Pierre Croisille
Department of Mathematics
University of Metz
Metz, France
email: croisil@poncelet.univ-metz.fr

Dalia Fishelov
Tel-Aviv Academic College of Engineering
218 Bnei-Efraim St., Tel-Aviv 69107, Israel
and School of Mathematical Sciences
Tel Aviv University
Ramat Aviv, Tel Aviv 69978, Israel
email: daliaf@post.tau.ac.il

Shlomo Trachtenberg
Department of Membrane and Ultrastructure Research
The Hebrew University-Hadassah Medical School
P.O. Box 12271, Jerusalem 91120, Israel
email: shlomot@cc.huji.ac.il

November 9, 2004

Abstract. A pure-streamfunction formulation is introduced for the numerical simulation of the two-dimensional incompressible Navier-Stokes equations. The idea is to replace the vorticity in the vorticity- streamfunction evolution equation by the Laplacian of the streamfunction. The resulting formulation includes the streamfunction only, thus no inter-function relations need to be invoked. A compact numerical scheme, which interpolates streamfunction values as well as its first order derivatives, is presented and analyzed. A number of numerical experiments are presented, including driven and double driven cavities, where the Reynolds numbers are sufficiently large, leading to symmetry breaking of asymptotic solutions.

Keywords: Navier-Stokes equations, streamfunction formulation, vorticity, numerical algorithm, compact schemes, driven cavity, symmetry breaking, asymptotic behavior.

1 Introduction

A new methodology for tracking vorticity dynamics was introduced in [3], [12]. More specifically, we studied the time evolution of the planar flow subject to the Navier-Stokes equations. It is the purpose of the present paper to upgrade this methodology by further reducing the role of vorticity and concentrating on the streamfuction instead.

We recall the basic setup. Let $\Omega \subseteq R^2$ be a bounded, simply connected domain with smooth boundary $\partial\Omega$. An incompressible, viscid flow in Ω is governed by the Navier-Stokes equations [21] (in its "vorticity-velocity" formulation)

$$\partial_t \xi + (\mathbf{u} \cdot \nabla)\xi = \nu \Delta \xi \quad \text{in } \Omega, \tag{1.1}$$

$$\nabla \cdot \mathbf{u} = \mathbf{0} \quad \text{in } \Omega. \tag{1.2}$$

The system (1.1-1.2) expresses the evolution of the vorticity $\xi = \partial_x v - \partial_y u$, where $\mathbf{u} = (u, v)$ is the velocity (and (x, y) are the coordinates in Ω). The coefficient $\nu > 0$ is the viscosity coefficient.

The system (1.1-1.2) is supplemented by the initial data

$$\xi_0(x, y) = \xi(x, y, t)|_{t=0}, \quad (x, y) \in \Omega, \tag{1.3}$$

and a boundary condition on $\partial\Omega$. Indeed, as has been discussed in [3], this condition is the "source of (numerical and theoretical) trouble", since it is normally expressed in terms of the **velocity**, rather than the **vorticity**. In our presentation here we take the most common condition, the so-called "no-slip" condition,

$$\mathbf{u}(x, y, t) = \mathbf{0} \quad \text{for } (x, y) \in \partial\Omega \quad \text{and all } t \geq 0. \tag{1.4}$$

The difficulty of "translating" (1.4) to a boundary condition adequate for use in (1.1-1.2) is a major topic of any numerical simulation. In this paper we overcome this difficulty by transforming the system (1.1-1.2) to the "pure streamfunction" version. It will also be clear how to replace the boundary condition (1.4) by more general ones. In fact, most of our numerical examples in this paper are studied in this more general case.

The vorticity formulation (1.1-1.2) has been the starting point for a wide variety of methods designed to solve numerically the Navier-Stokes equations. Here we mention two of them, which are of particular relevance to the present paper. In fact, each one of them can be regarded as a "family" of algorithms, which share some common basic structural hypotheses, yet differ considerably in their technical details. The first is generally labeled as the "vortex method". It consists of a wide array of algorithms, all based on the approximation of the vorticity field by a collection of "singular objects" (such as point vortices, vortex filaments etc.). These objects (which are often mathematically "regularized") are advected and diffused in a way which preserves the main physical features of the flow. Clearly, the generation of vorticity on the boundary is of crucial significance in this approach. We refer the reader to the recent book [6] for a comprehensive treatment. The second method is usually referred to as the "vorticity-streamfunction" method, and has gained increasing attention in recent years (see e.g. [8], [7], [18], [22], [4], [15], [14]). In some sense the streamfunction-vorticity formulation is an evolution of vortex methods. However, while the latter is a "particle method", which does not require a grid, the former assumes a smooth distribution of vorticity laid out on a regular grid. The vorticity equation (1.1) is then treated by temporal discretization. Once again, there are numerous ways of handling the spatial discretization, such as spectral techniques, finite differences, finite volume or finite element algorithms. The velocity field is typically updated, subject to the incompressibility constraint (1.2), by means of the evolution of the streamfunction (see Section 2 below for some mathematical background). Consider for example, the recent paper [4], where the evolution of the vorticity is accomplished by a "fractional step scheme". The first step ("hyperbolic") takes care of the advection. The second step, which is labeled there as a "Stokes flow step", is a "parabolic-elliptic" system, where the vorticity is diffused by a heat-type equation, coupled to a Poisson equation which ties the vorticity to the streamfunction. Since the Poisson equation allows for only one boundary condition on the streamfunction (say, of Dirichlet type), the second one (see Section 2 below for details) must be accommodated by accounting appropriately for the vorticity boundary values. Thus, boundary conditions for the vorticity must be brought into play. This approach should be compared with Gresho's observation ([11, pp 428, 429]), that "there are no boundary conditions for the vorticity, and none is needed" hence "the elliptic equation for the streamfunction cannot be viewed in isolation because the inevitable conclusion is that it carries too many boundary conditions". This "overdeterminacy" problem was addressed in the previous paper [3]. The key idea of "vorticity projection" was introduced; instead of solving the Poisson equation $\xi = \Delta\psi$ (which, as already observed, cannot take care of the two conditions on ψ) one solves $\Delta\xi = \Delta^2\psi$. The two boundary conditions are applied directly to ψ, and there is no need for boundary values of the vorticity. This idea is carried one step further in this paper (compare [12]). The vorticity "disappears" altogether and only the streamfunction and its gradient (i.e., velocity) are discretized in a "box-scheme" style. This means that all discretized values are attached to the grid nodes. The gradient values (which are regarded independently) are related to the function values via suitable compatibility conditions, preserving the overall accuracy of the scheme. We are therefore justified in labeling the scheme presented here as a "pure streamfunction" scheme, which follows closely the theoretical treatment of Eq. (1.1-1.2).

The plan of the paper is as follows. In section 2 we recall the classical construction of the streamfunction and present the mathematical background needed for our treatment. A basic element in this study consists of using the bilaplacian Δ^2 as the "driving generator" of the evolution. In section 3 we describe our numerical scheme, where the spatial discretization of Δ^2 plays a significant role. Briefly, we assign, at each node, values for the streamfunction and its gradient, and use a compact (second-order) scheme for Δ^2. It allows a "clean" representation of the boundary condition, restricted fully to the boundary points. Section 4 is devoted to a detailed study of questions of stability and convergence in a suitable linearized model. In section 5 we present detailed results of numerical experiments, including a driven and a doubly-driven cavity. Here we go beyond the mere inspection of the time evolution and study also aspects of asymptotic behavior and "breakdown of symmetry" [3], [17].

The present scheme, as well as some numerical results, have been presented by three of the authors at a conference (see [9]).

2 Pure-Streamfunction Formulation.

The streamfunction $\psi(x, y, t)$ was already introduced by Lagrange (see [13]) as a prime object in the investigation of the two-dimensional incompressible flow. The incompressibility condition (1.2) entails the existence of a function $\psi(x, y, t)$ such that, for any fixed $t \geq 0$,

$$\mathbf{u}(\mathbf{x}, t) = \nabla^{\perp}\psi = (-\frac{\partial \psi}{\partial y}, \frac{\partial \psi}{\partial x}). \tag{2.1}$$

It follows that $\xi = \Delta\psi$ and equation (1.1) takes the form

$$\partial_t(\Delta\psi) + (\nabla^{\perp}\psi) \cdot \nabla(\Delta\psi) = \nu\Delta^2\psi, \quad \text{in } \Omega. \tag{2.2}$$

Observe that the velocity field $\mathbf{u}$ is divergence-free due to (2.1). Furthermore, the boundary condition (1.4) now reads

$$\nabla\psi(x, y, t) = \mathbf{0} \quad \text{for } (x, y) \in \partial\Omega, \quad t \geq 0. \tag{2.3}$$

Since ψ is clearly only determined up to an additive constant, we can rewrite (2.3) as

$$\psi(x, y, t) = \frac{\partial \psi}{\partial n}(x, y, t) = 0, \quad (x, y) \in \partial\Omega, \quad t \geq 0, \tag{2.4}$$

where $\frac{\partial}{\partial n}$ is the outward normal derivative. Finally, the initial data (1.3) is now written in terms of ψ,

$$\psi_0(x, y) = \psi(x, y, t)|_{t=0}, \quad (x, y) \in \Omega. \tag{2.5}$$

For functions ψ which are sufficiently regular the boundary condition (2.4) is equivalent to

$$\psi(x, y, t) \in H_0^2(\Omega) \quad \text{for any fixed} \quad t \geq 0, \tag{2.6}$$

where H^2 is the Sobolev space of order 2, equipped with the norm

$$\|\psi(\cdot,\cdot,t)\|_{H^2}^2 = \int_\Omega \psi^2 dxdy + \int_\Omega (\Delta\psi)^2 dxdy \tag{2.7}$$

(see [16]). The closed subspace $H_0^2(\Omega) \subseteq H^2(\Omega)$ is defined as the closure of the subspace C_0^∞ of smooth compactly-supported functions, with respect to the H^2-norm.

The Sobolev space H^4 is defined in exactly the same fashion, adding the integral of $(\Delta^2\psi)^2$ to the right-hand-side of (2.7). As is well-known, the operator Δ^2 is a positive (self-adjoint) operator in H^4 [16], whose domain is $H^4 \cap H_0^2$. It therefore gives rise to a contraction (analytic) semigroup which solves (uniquely) the linear equation

$$\partial_t(\Delta\Theta) = \nu\Delta^2\Theta, \quad \Theta(\cdot,\cdot,t) \in H_0^2(\Omega). \tag{2.8}$$

Observe the presence of $\Delta\Theta$ in the left-hand-side of (2.8). It makes the equation more subtle than a simple generalization of the heat equation. For example, a "formal division" by Δ might lead one to conclude that the "spatial order" of the equation is two, hence (in analogy with the heat equation) only **one** boundary condition is needed (i.e., $\Theta \in H_0^1$). This is in fact not the case, and a double condition (i.e., H_0^2, as in (2.4) is needed. Even the definition of "eigenfunctions" for (2.8) (and their completeness) is not quite clear. We refer to [12] for the one dimensional case (where $\Omega \subseteq R$ is an interval).

Comparing Eqs. (2.2) and (2.8) we see that the convective nonlinear term in (2.2) adds yet another difficulty to the mathematical study of the equation. Furthermore, an important objective of this study is the extension of the theory to "rough" initial data, namely, letting $\xi_0 = \Delta\psi_0$ be a singular function. This is not only a "pure mathematical interest" but, on the contrary, represents the common physical (and numerical) models of point vortices or vortex filaments. We refer the reader to [2] for a full treatment of the mathematical aspects. We emphasize that our "pure streamfunction" approach in this paper is very closely linked to the theoretical treatment. In what follows we indicate how the questions of uniqueness and asymptotic decay are handled in this framework. The results of the two theorems are certainly not new, but their proofs in terms of the streamfunction shed light on the usefulness of this formulation. Furthermore, they are very close to the proofs in the discrete case. In particular, the estimates used in the proof of Theorem 2.1 are analogous to the stability proof for the convergence of the discrete scheme in Theorem 4.1.

Theorem 2.1 (Uniqueness) *Let $\psi, \tilde{\psi} \in H_0^2(\Omega)$ be solutions of (2.2- 2.4) having the same initial data. Let $\mathbf{u} = \nabla^\perp\psi$, $\mathbf{v} = \nabla^\perp\tilde{\psi}$ be the corresponding velocity fields, and $\xi = \Delta\psi$, $\eta = \Delta\tilde{\psi}$ the corresponding vorticities. Then $\psi \equiv \tilde{\psi}$.*

Proof. We consider equation (1.1) and the corresponding one for $\eta, \mathbf{v}$. Taking their difference and multiplying by $\psi - \tilde{\psi}$ we get,

$$\begin{array}{c} \int_\Omega(\psi-\tilde{\psi})\partial_t(\xi-\eta)d\mathbf{x} - \int_\Omega \xi((\mathbf{u}-\mathbf{v})\cdot\nabla)(\psi-\tilde{\psi})d\mathbf{x} \\ -\int_\Omega(\xi-\eta)(\mathbf{v}\cdot\nabla)(\psi-\tilde{\psi})d\mathbf{x} = \nu\int_\Omega(\xi-\eta)^2 d\mathbf{x}. \end{array} \tag{2.9}$$

But clearly $(\mathbf{u}-\mathbf{v})\cdot\nabla(\psi-\tilde{\psi}) \equiv 0$. The first term in the LHS of (2.9) can be rewritten as

$$\int_\Omega(\psi-\tilde{\psi})\partial_t(\xi-\eta)d\mathbf{x} = -\frac{1}{2}\frac{d}{dt}\int_\Omega|\nabla(\psi-\tilde{\psi})|^2 d\mathbf{x}. \tag{2.10}$$

As for the third integral in the LHS of (2.9), we use Hölder's inequality, an interpolation inequality for the L_4 norm (see [21], Sec. 3.3.3) and standard elliptic estimates to obtain

$$\begin{array}{l} |\int_\Omega (\xi-\eta)(\mathbf{v}\cdot\nabla)(\psi-\tilde{\psi})d\mathbf{x}| \le \|\xi-\eta\|_{L^2(\Omega)}\ \|\mathbf{v}\|_{L^4(\Omega)}\ \|\nabla(\psi-\tilde{\psi})\|_{L^4(\Omega)} \\ \le C\|\xi-\eta\|_{L^2(\Omega)}\ \|\mathbf{v}\|^{1/2}_{L^2(\Omega)}\ \|\nabla\mathbf{v}\|^{1/2}_{L^2(\Omega)}\ \|\nabla(\psi-\tilde{\psi})\|^{1/2}_{L^2(\Omega)}\ \|\Delta(\psi-\tilde{\psi})\|^{1/2}_{L^2(\Omega)} \end{array} \tag{2.11}$$

(where C is a "generic" constant depending only on Ω). We now note that, by definition,

$$\|\mathbf{v}\|_{L^2(\Omega)} \le C\|\tilde{\psi}\|_{H^1_0(\Omega)} \le C[\|\tilde{\psi}\|_{L^2(\Omega)} + \|\Delta\tilde{\psi}\|_{L^2(\Omega)}],$$

$$\|\nabla\mathbf{v}\|_{L^2(\Omega)} \le C[\|\tilde{\psi}\|_{L^2(\Omega)} + \|\Delta\tilde{\psi}\|_{L^2(\Omega)}],$$

hence (2.11) can be rewritten as,

$$\begin{array}{c} |\int_\Omega (\xi-\eta)(\mathbf{v}\cdot\nabla)(\psi-\tilde{\psi})d\mathbf{x}| \le \\ C\{\|\xi-\eta\|^{3/2}_{L^2(\Omega)}\ \|\nabla(\psi-\tilde{\psi})\|^{1/2}_{L^2(\Omega)}[\|\tilde{\psi}\|_{L^2(\Omega)} + \|\Delta\tilde{\psi}\|_{L^2(\Omega)}]\}. \end{array} \tag{2.12}$$

The RHS in (2.12) can be further estimated by

$$\begin{array}{c} \|\xi-\eta\|^{3/2}_{L^2(\Omega)}\ \|\nabla(\psi-\tilde{\psi})\|^{1/2}_{L^2(\Omega)}[\|\tilde{\psi}\|_{L^2(\Omega)} + \|\Delta\tilde{\psi}\|_{L^2(\Omega)}] \\ \le \epsilon\|\xi-\eta\|^2_{L^2(\Omega)} + \frac{64}{81\epsilon^3}[\|\tilde{\psi}\|_{L^2(\Omega)} + \|\Delta\tilde{\psi}\|_{L^2(\Omega)}]^4\ \|\nabla(\psi-\tilde{\psi})\|^2_{L^2(\Omega)}. \end{array} \tag{2.13}$$

We take $\epsilon = \frac{\nu}{2C}$ in this estimate and insert it in (2.9). In conjunction with (2.10), (2.12) we get,

$$\frac{d}{dt}\|\nabla(\psi-\tilde{\psi})\|^2_{L^2(\Omega)} \le C\|\nabla(\psi-\tilde{\psi})\|^2_{L^2(\Omega)}, \tag{2.14}$$

where $C>0$ depends on $\tilde{\psi}$ (in addition to ν, Ω) but not on ψ. Since $\psi(\mathbf{x},0)=\tilde{\psi}(\mathbf{x},0)$, the Gronwall inequality yields $\psi\equiv\tilde{\psi}$. ■

Turning to the asymptotic behavior of the solution to (2.2), we have the following.

Theorem 2.2 (Decay of solutions) *Let $\psi(\mathbf{x},t)$ be a solution to (2.2). Then there exists a positive constant λ, depending only on Ω, such that*

$$\||\nabla\psi(\mathbf{x},t)|\|_{L^2(\Omega)} \le e^{-\nu\lambda t}\||\nabla\psi(\mathbf{x},0)|\|_{L^2(\Omega)}. \tag{2.15}$$

Proof. Let us first note that

$$\int_\Omega \frac{\partial\Delta\psi}{\partial t}\psi d\mathbf{x} = \frac{1}{2}\frac{d}{dt}\int_\Omega \psi\Delta\psi d\mathbf{x}. \tag{2.16}$$

We may rewrite the integral in RHS of (2.16) as follows.

$$\int_\Omega \psi\Delta\psi d\mathbf{x} = \int_\Omega \psi\nabla\cdot(\nabla\psi) = -\int_\Omega |\nabla\psi|^2 d\mathbf{x}. \tag{2.17}$$

Combining equations (2.16-2.17) and (2.2), we find that

$$-\frac{1}{2}\frac{\partial}{\partial t}\int_\Omega |\nabla\psi|^2 d\mathbf{x} = -\int_\Omega \psi(\nabla^\perp\psi\cdot\nabla)\Delta\psi d\mathbf{x} + \nu\int_\Omega \psi\Delta^2\psi d\mathbf{x}. \tag{2.18}$$

Using (2.1), the first term in the RHS of (2.18) may be rewritten as follows.

$$\int_\Omega \psi(\mathbf{u}\cdot\nabla)\Delta\psi d\mathbf{x} = -\int_\Omega (\nabla\psi\cdot\mathbf{u})\Delta\psi d\mathbf{x} = 0, \tag{2.19}$$

since $\nabla\psi\cdot\mathbf{u}\equiv 0$.

Now, we treat the second term in the RHS of (2.18). Since Δ is a self-adjoint operator on $H_0^2(\Omega)$,

$$\int_\Omega \psi\Delta^2\psi = \int_\Omega (\Delta\psi)^2 d\mathbf{x}. \tag{2.20}$$

Applying (2.19-2.20) to (2.18), we find that

$$\frac{1}{2}\frac{\partial}{\partial t}\int_\Omega |\nabla\psi|^2 d\mathbf{x} = -\nu\int_\Omega (\Delta\psi)^2 d\mathbf{x}.$$

Using the Poincaré inequality

$$\int_\Omega (\Delta\psi)^2 d\mathbf{x} \geq \lambda\int_\Omega |\nabla\psi|^2 d\mathbf{x},$$

where λ is a positive constant depending on Ω, we conclude that

$$\||\nabla\psi(\mathbf{x},t)|\|_{L^2(\Omega)} \leq e^{-\nu\lambda t}\||\nabla\psi(\mathbf{x},0)|\|_{L^2(\Omega)}.$$

■

3 The Numerical Scheme.

To simplify the exposition, assume that Ω is a rectangle $[a,b]\times[c,d]$. We lay out a uniform grid $a\leq x_0 < x_1 < ... < x_N = b$, $c\leq y_0 < y_1 < ... < y_M = d$. Assume that $\Delta x = \Delta y = h$. At each grid point (x_i, y_j) we have three unknowns $\psi_{ij}, p_{ij}, q_{ij}$, where $p = \psi_x$ and $q = \psi_y$.

The time discretization is obtained by a Crank-Nicolson scheme, which approximates (2.2). The latter is applied at interior points $1\leq i\leq N-1, 1\leq j\leq M-1$. On the boundary $i = 0, N$ or $j = 0, M$ $\psi, p = \psi_x, q = \psi_y$ are determined by the boundary conditions (2.4). In order to do that we have to give discrete expressions for the spatial operators which appear in (2.2).

3.1 Spatial Discretization.

3.1.1 The Viscous Term.

Our scheme is based on Stephenson's [20] scheme for the biharmonic equation

$$\Delta^2\psi = f.$$

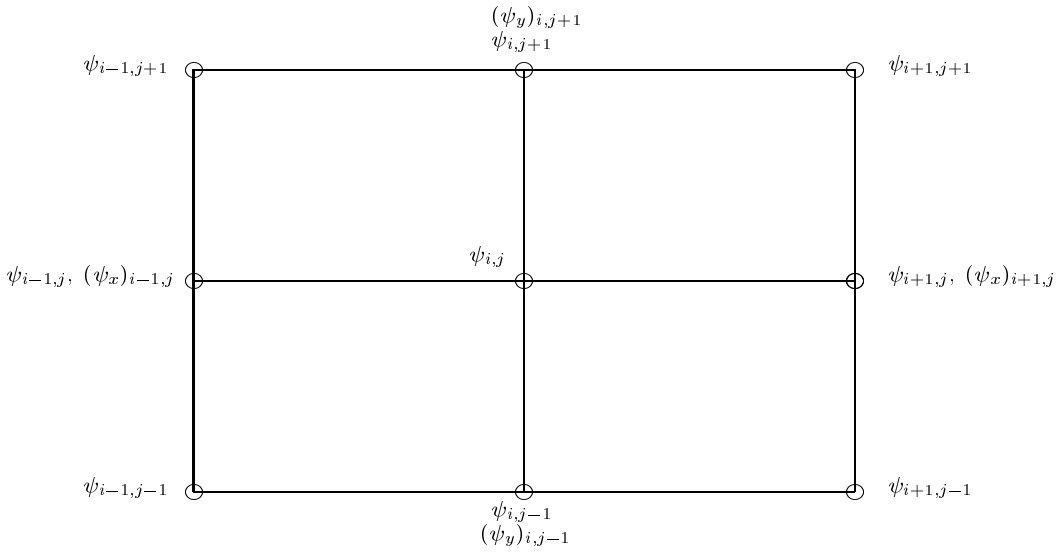

Figure 1: Stephenson's scheme for $\Delta^2\psi = f$: The finite difference operator $(\Delta_h^2)^c\psi$ at point (i,j) is $\Delta^2 P(x_i, y_j)$ where $\psi = P(x,y)$ is a polynomial in $P^3 + \mathrm{Span}(x^4, x^2y^2, y^4)$ defined by the 13 collocated values for ψ, ψ_x, ψ_y displayed.

Later on, Altas *et al.* [1] and Kupferman [12] applied Stephenson's scheme, using a multigrid solver. Stephenson's compact approximation for the biharmonic operator is the following.

$$
\left\{
\begin{array}{ll}
(\Delta_h^2)^c\psi_{i,j} & = \dfrac{1}{h^4}\Big\{56\psi_{i,j} - 16(\psi_{i+1,j} + \psi_{i,j+1} + \psi_{i-1,j} + \psi_{i,j-1}) \\
& \quad +2(\psi_{i+1,j+1} + \psi_{i-1,j+1} + \psi_{i-1,j-1} + \psi_{i+1,j-1}) \\
& \quad +6h[(\psi_x)_{i+1,j} - (\psi_x)_{i-1,j} + (\psi_y)_{i,j+1} - (\psi_y)_{i,j-1}]\Big\} \\
& = f_{i,j}
\end{array}
\right. \tag{3.1}
$$

Here, $(\Delta_h^2)^c\psi_{i,j}$ is the compact second-order approximation for $\Delta^2\psi$ specified in caption of Fig. 1. We have also to relate ψ_x and ψ_y to ψ. This is done via the following fourth-order compact schemes.

$$
h(\psi_x)_{i,j} = \frac{3}{4}(\psi_{i+1,j} - \psi_{i-1,j}) - \frac{h}{4}\big[(\psi_x)_{i+1,j} + (\psi_x)_{i-1,j}\big] \tag{3.2}
$$

$$
h(\psi_y)_{i,j} = \frac{3}{4}(\psi_{i,j+1} - \psi_{i,j-1}) - \frac{h}{4}\big[(\psi_y)_{i,j+1} + (\psi_y)_{i,j-1}\big] \tag{3.3}
$$

Equations (3.1-3.3) form a second order compact scheme for $\Delta^2\psi$, involving values of ψ, ψ_x and ψ_y at (i,j) and at its eight nearest neighbors (see Figure 1). Thus, the scheme is compact. The approximation above is applied at any interior point $1 \le i \le N-1, 1 \le j \le M-1$. On the boundary $i = 0, N$ or $j = 0, M$ ψ, ψ_x, ψ_y are determined from the boundary conditions (2.4).

3.1.2 The Laplacian of a Discrete Function.

For any function g we define the discrete approximation to Δg by $\Delta_h g$, where $\Delta_h g$ is

$$\Delta_h g = \delta_x^2 g + \delta_y^2 g, \tag{3.4}$$

and

$$\delta_x^2 g_{i,j} = \frac{g_{i+1,j} - 2g_{i,j} + g_{i-1,j}}{h^2} \quad , \quad \delta_y^2 g_{i,j} = \frac{g_{i,j+1} - 2g_{i,j} + g_{i,j-1}}{h^2}.$$

3.1.3 The Convective Term.

The convective term $(\nabla^\perp \psi) \cdot \nabla(\Delta\psi)$ is approximated as follows.

$$(\nabla^\perp \psi)_{i,j} = \big[-(\psi_y)_{i,j}, (\psi_x)_{i,j} \big]. \tag{3.5}$$

No further approximation is needed, since ψ_x and ψ_y are part of the unknowns in our discretization. Now,

$$\nabla(\Delta\psi)_{i,j} = ((\Delta\psi_x)_{i,j}, (\Delta\psi_y)_{i,j}) = \ = ((\Delta_h\psi_x)_{i,j}, (\Delta_h\psi_y)_{i,j}) + O(h^2, h^2). \tag{3.6}$$

Note that the above discretization is well defined for any interior point $1 \le i \le N-1, 1 \le j \le M-1$. The resulting scheme has the following form.

3.2 The Scheme

Combining (3.1-3.6) and the time discretization, we obtain the following scheme.

$$\begin{cases} \dfrac{(\Delta_h\psi_{i,j})^{n+1/2} - (\Delta_h\psi i,j)^n}{\Delta t/2} = \\ -[-(\psi_y^n)_{i,j}, (\psi_x^n)_{i,j}] \cdot [(\Delta_h\psi_x^n)_{i,j}, (\Delta_h\psi_y^n)_{i,j}] \\ +\dfrac{\nu}{2}\big[(\Delta_h^2)^c\psi_{i,j}^{n+1/2} + (\Delta_h^2)^c\psi_{i,j}^n\big] \end{cases} \tag{3.7}$$

$$\begin{cases} \dfrac{(\Delta_h\psi_{i,j})^{n+1} - (\Delta_h\psi i,j)^n}{\Delta t} = \\ -[-(\psi_y^{n+1/2}]_{i,j}, [\psi_x^{n+1/2})_{i,j}] \cdot [(\Delta_h\psi_x^{n+1/2})_{i,j}, (\Delta_h\psi_y^{n+1/2})_{i,j}] \\ +\dfrac{\nu}{2}[(\Delta_h^2)^c\psi_{i,j}^{n+1} + (\Delta_h^2)^c\psi_{i,j}^n] \end{cases} \tag{3.8}$$

where $(\Delta_h^2)^c$ is defined in (3.1).

Remark that we apply the scheme above to all interior point, and on boundary points we impose the boundary conditions by determining ψ, ψ_x and ψ_y from (2.4).

4 Stability and Convergence in Two Dimensions

4.1 Stability of the Predictor-Corrector scheme in Two Dimensions

We consider the predictor-corrector scheme (3.7)-(3.8) applied to the linear model equation

$$\Delta\psi_t = a\Delta\psi_x + b\Delta\psi_y + \nu\Delta^2\psi. \tag{4.1}$$

This scheme reads

$$(4.2)\quad \begin{cases} \dfrac{\Delta_h\psi^{n+1/2}-\Delta_h\psi^n}{\Delta t/2} = a\Delta_h\psi_x^n + b\Delta_h\psi_y^n + \dfrac{\nu}{2}(\Delta_h^2\psi^n + \Delta_h^2\psi^{n+1/2}) \quad (a) \\ \dfrac{\Delta_h\psi^{n+1}-\Delta_h\psi^n}{\Delta t} = a\Delta_h\psi_x^{n+1/2} + b\Delta_h\psi_y^{n+1/2} + \dfrac{\nu}{2}(\Delta_h^2\psi^{n+1} + \Delta_h^2\psi^n) \quad (b) \end{cases}$$

where $\Delta_h\psi^n$, $\Delta_h^2\psi^n$, ψ_x^n and ψ_y^n are defined in (3.4) and (3.1-3.3) respectively. Denote

$$(4.3)\qquad \eta = \frac{\Delta t}{h} \quad ; \quad \mu = \frac{\nu\Delta t}{h^2}$$

We have

Proposition 4.1 *The difference scheme (4.2) is stable in the Von Neumann sense under the sufficient condition*

$$(4.4)\qquad \max(|a|,|b|)\ \eta \le \min(\frac{\sqrt{8}}{3}\sqrt{\mu}, \frac{\sqrt{2}}{3})$$

Proof:
Let $\theta = \alpha h \in [0, 2\pi[$, $\phi = \beta h \in [0, 2\pi[$ and $\psi_{jk}^n = \widehat{\psi^n}(\alpha,\beta)e^{ij\theta}e^{ik\phi}$. We denote by $g_1(\theta,\phi)$ the amplification factor of the predictor step (4.2_a), $g_2(\theta,\phi)$ the amplification factor after the two steps (4.2). The factor $g_1(\theta,\phi)$ is

$$(4.5)\qquad g_1(\theta,\phi) = \frac{A_1(\theta,\phi) - B_1(\theta,\phi) + iC_1(\theta,\phi)}{A_1(\theta,\phi) + B_1(\theta,\phi)}$$

with

$$A_1(\theta,\phi) = \frac{2-2\cos\theta}{h^2} + \frac{2-2\cos\phi}{h^2},$$

$$B_1(\theta,\phi) = \frac{\mu}{4}\big[6\frac{2-2\cos\theta}{h^2}\frac{1-\cos\theta}{2+\cos\theta} + 6\frac{2-2\cos\phi}{h^2}\frac{1-\cos\phi}{2+\cos\phi} + 2\frac{2-2\cos\theta}{h}\frac{2-2\cos\phi}{h}\big],$$

$$C_1(\theta,\phi) = \frac{\eta}{2}\big[\frac{2-2\cos\theta}{h^2} + \frac{2-2\cos\phi}{h^2}\big]\big[\frac{3a\sin(\theta)}{2+\cos\theta} + \frac{3b\sin(\phi)}{2+\cos\phi}\big].$$

The factor $g_2(\theta,\phi)$ is

$$(4.6)\qquad g_2(\theta,\phi) = \frac{A_1(\theta,\phi) - 2B_1(\theta,\phi) + 2iC_1(\theta,\phi)g_1(\theta,\phi)}{A_1(\theta,\phi) + 2B_1(\theta,\phi)}$$

The stability condition $\sup_{\theta,\phi}|g_2(\theta,\phi)| \le 1$ is equivalent for each $\theta,\phi \in [0,2\pi[$ to

$$(4.7)\qquad \begin{aligned} &-4C_1(\theta,\phi)\,\mathrm{Im}(g_1(\theta,\phi))[A_1(\theta,\phi) - 2B_1(\theta,\phi)] + 4C_1^2(\theta,\phi)|g_1(\theta,\phi)|^2 \\ &\le 8A_1(\theta,\phi)B_1(\theta,\phi). \end{aligned}$$

We restrict ourselves to the case where

$$\sup_{\theta,\phi\in[0,2\pi[} |g_1(\theta,\phi)| \leq 1 \tag{4.8}$$

A sufficient condition for (4.8) to be satisfied is

$$\max(|a|,|b|)\eta \leq \frac{\sqrt{8}}{3}\sqrt{\mu}.$$

Then (4.7) is satisfied under the sufficient condition

$$C_1^2\big[1-\frac{A_1-2B_1}{A_1+B_1}\big] \leq 2A_1B_1.$$

The latter is equivalent to

$$\frac{1}{4}\eta^2\big[\frac{3a\sin(\theta)}{2+\cos\theta}+\frac{3b\sin(\phi)}{2+\cos\phi}\big]^2\cdot 3\frac{A_1}{A_1+B_1} \leq 2. \tag{4.9}$$

A sufficient condition for (4.9) is

$$\max(a^2,b^2)\ \eta^2 \leq \frac{2}{9},$$

which completes the proof. ■

Observe that in the nonconvective case, $a=b=0$, the scheme is unconditionally stable, as could be expected. Thus, the presence of lower-order convective terms makes it necessary to limit the timestep.

Remark: Note that the restriction of the CFL number (4.4) by a formula of the type

$$\max(|a|,|b|)\ \eta \leq C\sqrt{\mu} \tag{4.10}$$

pertains to a centered scheme for the convection-diffusion equation, with an implicit discretization of the diffusive term and an explicit discretization of the convective term, even in the one-dimensional situation.

4.2 Convergence of the spatially semi-discrete two-dimensional scheme

In the next theorem, we prove a rate of convergence of h^2 for the time continuous version of scheme (3.7-3.8), when applied to the linear equation (4.1) on $[0,1]\times[0,1]$ in the H_0^2 setting.

Define $h=1/N, x_i=y_i=ih, 0\leq i\leq N$. We call $L^2_{h,0}$ the space of $N\times N$ arrays in x and y directions, for which $u_{0,j}=u_{N,j}=u_{i,0}=u_{i,N}=0$. For $u,v\in L^2_{0,h}$, the scalar product is

$$(u,v)_h=\sum_{i=1}^{N-1}\sum_{j=1}^{N-1}u_{ij}v_{ij}h^2$$

and the norm

$$|u|_h = (\sum_{i=1}^{N-1}\sum_{j=1}^{N-1} |u_{ij}|^2 h^2)^{1/2}$$

For $\tilde{\psi} \in L^2_{h,0}$, the spatial discrete operators $\Delta_h\tilde{\psi}$, $\Delta_h^2\tilde{\psi}$, $\tilde{\psi}_x$ and $\tilde{\psi}_y$ are defined in (3.4) and (3.1-3.3) respectively.
In the investigation of the convergence properties of our scheme we use the exact equation (2.2) and a semi-discrete analog of (3.7, 3.8). Thus the discrete solution is represented by the grid functions $\tilde{\psi}_{i,j}(t), \tilde{\psi}_{x,i,j}(t), \tilde{\psi}_{y,i,j}(t)$ which approximate the exact solution $\psi(x,y,t), \psi_x(x,y,t), \psi_y(x,y,t)$ at $(x,y) = (ih, jh)$. We have $\tilde{\psi}$, $\tilde{\psi}_x$, $\tilde{\psi}_y \in L^2_{h,0}$, so that the boundary values of $\tilde{\psi}$, $\tilde{\psi}_x$, $\tilde{\psi}_y$ vanish. Thus, the equation satisfied by the discrete functions is

$$\frac{\partial}{\partial t}\Delta_h\tilde{\psi} = a\Delta_h(\tilde{\psi}_x) + b\Delta_h(\tilde{\psi}_y) + \nu\Delta_h^2(\tilde{\psi}) \tag{4.11}$$

subject to initial conditions

$$\tilde{\psi}_{i,j} = \psi_0(ih, jh), \quad (\tilde{\psi}_x, \tilde{\psi}_y)_{i,j} = \big[\psi_{0,x}(ih, jh), \psi_{0,y}(ih, jh)\big]. \tag{4.12}$$

For every discrete $u \in L^2_{h,0}$ we set as usual

$$(\delta_x^+ u)_{i,j} = \frac{u_{i+1,j} - u_{i,j}}{h} \quad , \quad (\delta_y^+ u)_{i,j} = \frac{u_{i,j+1} - u_{i,j}}{h}. \tag{4.13}$$

and

$$(\delta_x u)_{i,j} = \frac{u_{i+1,j} - u_{i-1,j}}{2h} \quad , \quad (\delta_y u)_{i,j} = \frac{u_{i,j+1} - u_{i,j-1}}{2h}. \tag{4.14}$$

Our convergence result is the following.

Theorem 4.1 *Let the discrete solution $\tilde{\psi}, \tilde{\psi}_x, \tilde{\psi}_y$ satisfy (4.11), and the boundary conditions*

$$\tilde{\psi}_{i,j} = \tilde{\psi}_{x,i,j} = \tilde{\psi}_{y,i,j} = 0 \quad \textit{for } i \in \{0, N\} \textit{ or } j \in \{0, N\}.$$

Let ψ be the exact solution of (2.2) subject to the boundary conditions (2.4). Fix $\tau > 0$. Then, for $0 \le t \le \tau$, there exists a constant $C > 0$, depending only on τ and the initial data, such that

$$|e|_h + |\delta_x^+ e|_h + |\delta_y^+ e|_h \le Ch^2 \tag{4.15}$$

where $e = \tilde{\psi} - \psi$ is the difference between the approximate and the exact solutions on the grid, the latter being supposed sufficiently regular.

Proof. The exact solution ψ satisfies

$$\frac{\partial}{\partial t}\Delta_h\psi = a\Delta_h(\psi_x) + b\Delta_h(\psi_y) + \nu\Delta_h^2(\psi) - T, \tag{4.16}$$

where $T = O(h^2)$ is the truncation error. Observe that in (4.16), the values $(\psi_x)_{ij}, (\psi_y)_{ij}$ are not the components of the gradient of the given smooth solution ψ (at (i,j)) but

are the values obtained from the discrete values ψ_{ij} by use of (3.2-3.3). Subtracting (4.16) from (4.11) and denoting the error $e = \tilde{\psi} - \psi$, we have

$$\frac{\partial}{\partial t}\Delta_h e = a\Delta_h(e_x) + b\Delta_h(e_y) + \nu\Delta_h^2 e + T. \tag{4.17}$$

The viscous term given in (3.1) is

$$\begin{aligned}\nu\Delta_h^2 e_{ij} &= \frac{\nu}{h^4}\Big\{56e_{ij} - 16(e_{i+1,j} + e_{i-1,j}) - 16(e_{i,j+1} + e_{i,j-1}) \\ &+ 2(e_{i+1,j+1} + e_{i-1,j+1}) + 2(e_{i+1,j-1} + e_{i-1,j-1}) \\ &+ 6h[(e_x)_{i+1,j} - (e_x)_{i-1,j} + (e_y)_{i,j+1} - (e_y)_{i,j-1}]\Big\},\end{aligned}$$

which may be rewritten as

$$\begin{aligned}\nu\Delta_h^2 e_{ij} &= \frac{\nu}{h^4}\Big\{-8e_{ij} - 16(e_{i+1,j} - 2e_{ij} + e_{i-1,j}) - 16(e_{i,j+1} - 2e_{ij} + e_{i,j-1}) \\ &+ 2(e_{i+1,j+1} - 2e_{i,j+1} + e_{i-1,j+1}) + 2(e_{i+1,j-1} - 2e_{i,j-1} + e_{i-1,j-1}) \\ &+ 4(e_{i,j+1} + e_{i,j-1}) + 6h[(e_x)_{i+1,j} - (e_x)_{i-1,j} + (e_y)_{i,j+1} - (e_y)_{i,j-1}]\Big\}.\end{aligned}$$

The latter may be simplified to

$$\begin{aligned}&\nu\Delta_h^2 e_{ij} = \tfrac{\nu}{h^4}\Big\{-12h^2\delta_x^2 e_{ij} - 12h^2\delta_y^2 e_{ij} + 2h^4\delta_x^2\delta_y^2 e_{ij} + \\ &+6h[(e_x)_{i+1,j} - (e_x)_{i-1,j} + (e_y)_{i,j+1} - (e_y)_{i,j-1}]\Big\}.\end{aligned} \tag{4.18}$$

or

$$\nu\Delta_h^2 e_{i,j} = \nu\big[\delta_x^4 e_{i,j} + \delta_y^4 e_{i,j} + 2\delta_x^2\delta_y^2 e_{i,j}\big] \tag{4.19}$$

where

(4.20)

$$\delta_x^4 u_{i,j} = \frac{12}{h^2}\big[\delta_x(u_x)_{i,j} - \delta_x^2 u_{i,j}\big]\ ;\ \delta_y^4 u_{i,j} = \frac{12}{h^2}\big[\delta_y(u_y)_{i,j} - \delta_y^2 u_{i,j}\big]\ ;\ \delta_x^2\delta_y^2 u_{i,j} = (\delta_{xy})^2 u_{i,j}.$$

The rows (and the columns) of elements in $L^2_{h,0}$ are $(N+1)-$vectors $\theta = (\theta_0, \theta_1, ..., \theta_N)$ such that $\theta_0 = \theta_N = 0$. We denote by $l^2_{h,0}$ the $((N-1)-$dimensional) space of such vectors. It will be convenient to refer to the $(N-1)-$dimensional part $(\theta_1, ..., \theta_{N-1})$ of vectors in $l^2_{h,0}$ and the operators acting on it (with the understanding that $\theta_0 = \theta_N = 0$). The scalar product and the norm in $l^2_{h,0}$ are

$$(\theta, \tilde{\theta})_h = h\sum_{i=1}^{N-1}\theta_i\tilde{\theta}_i, \quad |\theta|_h^2 = h\sum_{i=1}^{N-1}\theta_i^2, \tag{4.21}$$

which is in agreement with the notation for $L^2_{h,0}$ (in the case of arrays).

The proof consists now of applying the energy method to (4.17). In order to do that, we need the discrete analog of the following $L^2(\Omega)$ scalar products denoted by $(\,.\,,\,.\,)$, where it is assumed that $\psi \in H_0^2(\Omega)$.

$$\begin{array}{ll} (i) & (\Delta\psi,\psi) = -|\nabla\psi|^2 \\ (ii) & (a\Delta\frac{\partial\psi}{\partial x} + b\Delta\frac{\partial\psi}{\partial y},\psi) = 0 \\ (iii) & (\Delta^2\psi,\psi) = |\Delta\psi|^2. \end{array} \tag{4.22}$$

The main difficulty is that the discrete gradient (e_x, e_y) in (4.17) is defined implicitly by (3.2)-(3.3), so that a classical discrete integration by parts like $(\delta_x e, e)_h = 0$ for $e \in l^2_{h,0}$ no longer holds. Also the biharmonic operator applied to e as defined by (3.1) involves the values of e_x. These values have to be related to the standard difference operators like $\delta_x^{\pm} e$ in order to get an equivalent form to (4.22(*iii*)).

Let us introduce P be as the finite difference operator acting in $l^2_{h,0}$ by

$$(P\theta)_i = \theta_{i-1} + 4\theta_i + \theta_{i+1}, \quad 1 \le i \le N-1, \quad \theta \in l^2_{h,0}. \tag{4.23}$$

The operator P is positive symmetric (diagonally dominated), so that by the Cauchy-Schwartz inequality,

$$2|\theta|_h^2 \le (P\theta,\theta)_h \le 6|\theta|_h^2, \quad \theta \in l^2_{h,0}. \tag{4.24}$$

Note that by (3.2), $(e_x)_{i,j}$ is defined by

$$(Pe_x)_{i,j} = \frac{3}{h}(e_{i+1,j} - e_{i-1,j}), \quad 1 \le i,j \le N-1. \tag{4.25}$$

In the sequel, we handle any grid function $u_{i,j} \in L^2_{h,0}$ as well as finite difference operators acting on them, as $(N-1)\times(N-1)$ matrices. Denoting $e_x^j = ((e_x)_{1,j},...,(e_x)_{N-1,j})^T$, $e^j = (e_{1,j},...,e_{N-1,j})^T$, $\quad ,1 \le j \le N-1$ the $j-th$ columns of the matrices e_x, e, we can rewrite (4.25) as

$$Pe_x^j = 6\delta_x e^j \quad , \quad 1 \le j \le N-1, \tag{4.26}$$

or simply in matrix form

$$Pe_x = 6\delta_x e, \tag{4.27}$$

and similarly

$$e_y P = 6\delta_y e. \tag{4.28}$$

Note that in (4.27-4.28), we refer to P as the symmetric positive definite matrix

$$P_{i,m} = \begin{cases} 4, & m = i \\ 1, & |m-i| = 1 \\ 0, & |m-i| \ge 2 \end{cases} \tag{4.29}$$

In addition, due to $(\delta_x u, u)_h = 0$ for $u \in l^2_{h,0}$, we have

$$(Pe_x^j, e^j)_h = 0 \quad , \quad j = 1,...,N-1. \tag{4.30}$$

Note also that multiplication on the left of a matrix A by P results in replacing its $i-$th row A^i by $4A^i + A^{i+1} + A^{i-1}$. Multiplication on the right has the same effect on the columns.
The matrix representing δ_x^2 is (see (3.4)) $h^{-2}(P - 6I)$, as multiplication on the left (of the matrix g), while δ_y^2 is expressed by the same multiplication on the right. Taking the scalar product of (4.17) with e yields

$$\left\{\begin{array}{lcll} (\frac{d}{dt}\Delta_h e, e)_h & = & \nu(\Delta_h^2 e, e)_h \qquad (I) \\ & + & a(\Delta_h e_x, e)_h + b(\Delta_h e_y, e)_h \qquad (II) \\ & + & (T, e)_h \qquad (III) \end{array}\right. \tag{4.31}$$

(I), (II), (III) are respectively the diffusive, convective, and truncation terms.

We first consider the diffusive term (I). The crucial step in the proof of the theorem is the derivation of a suitable lower bound for $(\Delta_h^2 e, e)_h$, for $e, e_x, e_y \in L^2_{h,0}(\Omega)$. In the continuous case, if $\phi \in H_0^2(\Omega)$, an integration by parts yields

$$(\Delta^2\phi, \phi)_{L^2(\Omega)} = \|\Delta\phi\|^2_{L^2(\Omega)}. \tag{4.32}$$

Our discrete analog is given by the following claim.
Claim: There exists a constant $C \geq 0$ independent of h, such that, for all grid functions $u \in L^2_{h,0}$

$$(\Delta_h^2 u, u)_h \geq C\left[|\delta_x^+ u_x|_h^2 + |\delta_y^+ u_y|_h^2 + |\delta_y^+ u_x|_h^2 + |\delta_x^+ u_y|_h^2\right], \tag{4.33}$$

where u_x, u_y are related to u as in (4.27), (4.28).

Proof of the claim: Let us first observe that for all $u, v \in l^2_{h,0}$

$$(\delta_x u, v)_h = (\delta_x^+ u, \Pi v)_h, \tag{4.34}$$

where $\Pi : l^2_{h,0} \to l^2_{h,0}$ is the averaging operator defined by

$$(\Pi v)_i = \frac{1}{2}(v_i + v_{i+1}), \quad 1 \leq i \leq N-1. \tag{4.35}$$

Indeed, to prove (4.34), we note that

$$(\delta_x u, v)_h = \frac{1}{2}\big((\delta_x^+ + \delta_x^-)u, v\big)_h. \tag{4.36}$$

But since $\delta_x^+ = \delta_x^- S$, where $(Sv)_k = v_{k+1}$, $1 \leq k \leq N-1$ is the forward shift in the x direction, we have
(4.37)

$$(\delta_x u, v)_h = -(u, \delta_x v)_h = -\left(\frac{1}{2}\delta_x^-(I+S)v, u\right)_h = \left(\frac{1}{2}(I+S)v, \delta_x^+ u\right)_h = (\Pi v, \delta_x^+ u)_h.$$

For any $u \in L^2_{h,0}$, we have now

$$\begin{array}{rcl} (\Delta_h^2 u, u)_h & = & (\delta_x^4 u, u)_h + (\delta_y^4 u, u)_h + 2(\delta_x^2\delta_y^2 u, u)_h \\ & = & \frac{12}{h^2}\left(\delta_x u_x - \delta_x^2 u, u\right)_h + \frac{12}{h^2}\left(\delta_y u_y - \delta_y^2 u, u\right)_h + 2\big(\delta_x^2\delta_y^2 u, u\big)_h. \end{array}$$

Next we check that for any $v \in l^2_{h,0}$

$$\frac{12}{h^2}\Big(\delta_x v_x - \delta_x^2 v, v\Big)_h \geq C|\delta_x^+ v_x|_h^2. \tag{4.38}$$

Noting (4.34) and $-(\delta_x^2 v, w)_h = (\delta_x^+ v, \delta_x^+ w)_h$ for all $v, w \in l^2_{h,0}$, we get

$$\begin{aligned}(\delta_x v_x - \delta_x^2 v, v)_h &= -(\delta_x^+ v, \Pi v_x)_h + (\delta_x^+ v, \delta_x^+ v)_h \\ &= (\delta_x^+ v, \delta_x^+ v - \Pi v_x)_h \\ &= (\delta_x^+ v - \Pi v_x, \delta_x^+ v - \Pi v_x)_h + (\Pi v_x, \delta_x^+ v - \Pi v_x)_h \\ &\geq (\Pi v_x, \delta_x^+ v - \Pi v_x)_h.\end{aligned}$$

Recall that $P = 6I + h^2\delta_x^2$. Then, by (4.27)

$$(v_x, z + \frac{h^2}{6}\delta_x^2 z)_h = \frac{1}{6}(v_x, Pz)_h = \frac{1}{6}(Pv_x, z)_h = (\delta_x v, z)_h = (\delta_x^+ v, \Pi z)_h, \quad z \in l^2_{h,0}. \tag{4.39}$$

Setting $z = v_x$ in (4.39), we have

$$(\Pi v_x, \delta_x^+ v - \Pi v_x)_h = (v_x, v_x + \frac{h^2}{6}\delta_x^2 v_x)_h - |\Pi v_x|_h^2 = |v_x|_h^2 - \frac{h^2}{6}|\delta_x^+ v_x|_h^2 - |\Pi v_x|_h^2. \tag{4.40}$$

Using finally that for all $w \in l^2_{h,0}$

$$|w|_h^2 - |\Pi w|_h^2 = \frac{h^2}{4}|\delta_x^+ w|_h^2, \tag{4.41}$$

we deduce from (4.40) that

$$(\delta_x v_x - \delta_x^2 v, v)_h \geq (\Pi v_x, \delta_x^+ v - \Pi v_x)_h = (\frac{h^2}{4} - \frac{h^2}{6})|\delta_x^+ v_x|_h^2 = \frac{h^2}{12}|\delta_x^+ v_x|_h^2, \tag{4.42}$$

which is the desired result (4.38). Clearly, the same result holds for a bidimensional grid function $v \in L^2_{h,0}$ (summation over all columns of the matrix v).
Consider now the mixed term $(\delta_x^2\delta_y^2 u, u)_h = |\delta_x^+\delta_y^+ u|_h^2$. We assert that

$$|\delta_x^+\delta_y^+ u|_h \geq \frac{1}{6}|\delta_x^+ u_y|_h. \tag{4.43}$$

To prove (4.43), we write first

$$\delta_x^+\delta_y^+ u_{i,j} = \frac{\delta_y^+ u_{i+1,j} - \delta_y^+ u_{i,j}}{h}. \tag{4.44}$$

Using $\delta_y^+ u_{i,j} = \delta_y u_{i,j} + \frac{h}{2}\delta_y^2 u_{i,j}$ and (4.28), we deduce

(4.45)

$$\left\{\begin{aligned}\delta_x^+\delta_y^+ u_{i,j} &= \frac{\delta_y u_{i+1,j} - \delta_y u_{i,j}}{h} + \frac{1}{2}\big[\delta_y^2 u_{i+1,j} - \delta_y^2 u_{i,j}\big] \\ &= \frac{1}{h}\big[(u_y)_{i+1,j} - (u_y)_{i,j}\big] + \frac{h}{6}\big[\delta_y^2(u_y)_{i+1,j} - \delta_y^2(u_y)_{i,j}\big] + \frac{1}{2}\big[\delta_y^2 u_{i+1,j} - \delta_y^2 u_{i,j}\big] \\ &= \delta_x^+(u_y)_{i,j} + \frac{h^2}{6}\delta_y^2\delta_x^+(u_y)_{i,j} + \frac{h}{2}\delta_y^2\delta_x^+ u_{i,j}.\end{aligned}\right.$$

In addition, using the definition of δ_y^2 we have

$$|\delta_y^2\delta_x^+ u_y|_h \leq \frac{4}{h^2}|\delta_x^+ u_y|_h, \tag{4.46}$$

and using $\delta_y^2 = \delta_y^-\delta_y^+$, we have again by definition

$$|\delta_y^2\delta_x^+ u|_h \leq \frac{2}{h}|\delta_y^+\delta_x^+ u|_h. \tag{4.47}$$

Therefore, we deduce from (4.45)

$$\begin{aligned} |\delta_x^+\delta_y^+ u|_h &\geq |\delta_x^+ u_y|_h - \frac{h^2}{6}|\delta_y^2\delta_x^+ u_y|_h - \frac{h}{2}|\delta_y^2\delta_x^+ u|_h \\ &\geq |\delta_x^+ u_y|_h - \frac{2}{3}|\delta_x^+ u_y|_h - |\delta_x^+\delta_y^+ u|_h. \end{aligned}$$

This gives finally $2|\delta_x^+\delta_y^+ u|_h \geq \frac{1}{3}|\delta_x^+ u_y|_h$ which is (4.43). We proceed in the same way in proving the symmetric estimate

$$|\delta_x^+\delta_y^+ u|_h \geq \frac{1}{6}|\delta_y^+ u_x|_h. \tag{4.48}$$

This concludes the proof of the claim (4.33).

The convective term $(II) = a(\Delta_h e_x, e)_h + b(\Delta_h e_y, e)_h$ in (4.31) is

$$(II) = a(\delta_x^2(e_x), e)_h + a(\delta_y^2(e_x), e)_h + b(\delta_x^2(e_y), e)_h + b(\delta_y^2(e_y), e)_h. \tag{4.49}$$

Since we do not have a strict discrete equivalent of (4.22(ii)) we proceed as follows. The first term in the right-hand-side of (4.49) is

$$a(\delta_x^2 e_x, e)_h = -a(\delta_x^+ e_x, \delta_x^+ e)_h. \tag{4.50}$$

so that

$$|a(\delta_x^2 e_x, e)_h| \leq |a|\left[\varepsilon|\delta_x^+ e_x|_h^2 + \frac{1}{4\varepsilon}|\delta_x^+ e|_h^2\right]. \tag{4.51}$$

where $\varepsilon > 0$ will be selected latter. Proceeding in the same way for the three other terms in (4.49), we find the estimate of the convective term

$$\begin{aligned} |a(\Delta_h e_x, e)_h &+ b(\Delta_h e_y, e)_h| \leq \max(|a|;|b|)\left[\varepsilon\{|\delta_x^+ e_x|_h^2 + |\delta_y^+ e_y|_h^2 + |\delta_x^+ e_y|_h^2 + |\delta_y^+ e_x|_h^2\}\right. \\ &+ \left.\frac{1}{2\varepsilon}\{|\delta_x^+ e|_h^2 + |\delta_y^+ e|_h^2\}\right]. \end{aligned}$$

Finally the truncation term (III) in (4.31) is estimated by

$$|(III)| = |(T, e)_h| \leq \frac{1}{2}|T|_h^2 + \frac{1}{2}|e|_h^2 \leq C'\left[h^4 + |\delta_x^+ e|_h^2 + |\delta_y^+ e|_h^2\right]. \tag{4.52}$$

Collecting now the terms (I),(II),(III) in (4.31), we find

$$\begin{aligned}\frac{1}{2}\frac{d}{dt}\left[|\delta_x^+ e|_h^2 + |\delta_y^+ e|_h^2\right] &= -(\frac{d}{dt}\Delta_h e, e)_h \\ &\leq \left[\varepsilon \max(|a|,|b|) - C\nu\right]\left[|\delta_x^+ e_x|_h^2 + |\delta_y^+ e_y|_h^2 + |\delta_x^+ e_y|_h^2 + |\delta_y^+ e_x|_h^2\right] \\ &+ \left[\frac{1}{2\varepsilon}\max(|a|,|b|) + C'\right]\left[|\delta_x^+ e|_h^2 + |\delta_y^+ e|_h^2\right] + C'h^4.\end{aligned}$$

Selecting now ε sufficiently small in order that $\left[\varepsilon \max(|a|;|b|) - C\nu\right] \leq 0$, we obtain

$$\frac{d}{dt}\left[|\delta_x^+ e|_h^2 + |\delta_y^+ e|_h^2\right] \leq C''(\nu,|a|,|b|)\left[|\delta_x^+ e|_h^2 + |\delta_y^+ e|_h^2 + h^4\right], \tag{4.53}$$

which gives the conclusion of the theorem for $|\delta_x^+ e|_h + |\delta_x^+ e|_h$ by the Gronwall inequality. The estimate for $|e|_h$ now follows from the discrete Poincaré inequality. ■.

Remark: Note that the error estimate (4.15) is directly linked to the truncation error $T = O(h^2)$.

5 Numerical Results

We present here several problems, towards which we applied our scheme. In the first test problem we take an exact solution to (2.2) (see[5]).

$$\psi(x,y,t) = -0.5e^{-2\nu t}\sin x \ \sin y, \quad 0 \leq x,y \leq \pi. \tag{5.1}$$

We have picked $\nu = 1$. Table 1 summarizes the error, e, and the relative error, e_r, where

$$e_{l_2} = \|\psi_{comp} - \psi_{exact}\|_{l^2},$$
$$e_r = e/\|\psi_{exact}\|_{l^2}$$

and

$$e_u = max|u_{comp} - u_{exact}|.$$

Here, ψ_{comp},u_{comp} and ψ_{exact},u_{exact} are the computed and the exact streamfunction and $x-$ component of the velocity field, respectively. We represent results for different time-levels and number of mesh points.

mesh		17×17	Rate	33×33	Rate	65×65
$t=1$	e_{l_2}	$2.437*10^{-5}$	4.05	$1.394*10^{-6}$	3.93	$9.114*10^{-8}$
	e_r	$2.134*10^{-4}$		$1.349*10^{-5}$		$8.371*10^{-7}$
	e_u	$2.797*10^{-5}$	4.00	$1.749*10^{-6}$	4.00	$1.093*10^{-7}$
$t=2$	e_{l_2}	$3.180*10^{-6}$	3.78	$2.322*10^{-7}$	4.07	$1.319*10^{-8}$
	e_r	$2.232*10^{-4}$		$1.334*10^{-5}$		$8.736*10^{-7}$
	e_u	$4.254*10^{-6}$	4.00	$2.663*10^{-7}$	4.00	$1.665*10^{-8}$
$t=3$	e_{l_2}	$4.289*10^{-7}$	3.97	$2.738*10^{-8}$	3.90	$1.831*10^{-9}$
	e_r	$2.235*10^{-4}$		$1.400*10^{-5}$		$8.750*10^{-7}$
	e_u	$6.199*10^{-7}$	4.00	$3.882*10^{-8}$	4.00	$1.677*10^{-9}$
$t=4$	e_{l_2}	$7.864*10^{-8}$	4.00	$4.925*10^{-9}$	4.27	$1.831*10^{-9}$
	e_r	$2.224*10^{-4}$		$1.400*10^{-5}$		$8.750*10^{-7}$
	e_u	$9.019*10^{-8}$	4.00	$5.648*10^{-9}$	4.00	$3.530*10^{-10}$

Table 1: Streamfunction formulation: Compact scheme for problem (1)- l_2 error, relative l_2 error and max error in the horizontal component of the velocity field.

Similar results are shown for the solution $\psi = e^{-t}(x^2+y^2)^2$ of the non-homogeneous problem

$$\frac{\partial(\Delta\psi)}{\partial t} + (\nabla^{\perp}\psi)\cdot\nabla(\Delta\psi) = \Delta^2\psi - 16e^{-t}(x^2+y^2+4),$$

for $0 \le x, y \le 1$. Table 2 displays the error, e, and the relative error, e_r, and e_u (the same quantities as in Table 1). We represent results for different time-levels and number of mesh points, and see that the convergence rate is around 2.

mesh		17×17	Rate	33×33	Rate	65×65
$t=0.25$	e_{l_2}	$6.202*10^{-5}$	1.986	$1.564*10^{-5}$	2.003	$3.903*10^{-6}$
	e_r	$8.176*10^{-5}$		$1.895*10^{-5}$		$4.535*10^{-6}$
	e_u	$2.070*10^{-4}$	1.986	$5.224*10^{-5}$	2.002	$1.304*10^{-5}$
$t=0.5$	e_{l_2}	$7.632*10^{-5}$	2.000	$1.908*10-5$	2.002	$4.762*10^{-6}$
	e_r	$1.030*10^{-4}$		$2.368*10^{-5}$		$5.671*10^{-6}$
	e_u	$2.572*10^{-4}$	2.000	$6.431*10^{-5}$	2.003	$1.605*10^{-5}$
$t=0.75$	e_{l_2}	$7.896*10^{-5}$	2.007	$1.964*10^{-5}$	2.002	$4.904*10^{-6}$
	e_r	$1.091*10^{-4}$		$2.498*10^{-5}$		$5.984*10^{-6}$
	e_u	$2.667*10^{-4}$	2.001	$6.664*10^{-5}$	2.008	$1.657*10^{-5}$
$t=1$	e_{l_2}	$7.818*10^{-5}$	2.007	$1.945*10^{-5}$	2.002	$4.856*10^{-6}$
	e_r	$1.110*10^{-4}$		$2.535*10^{-5}$		$6.072*10^{-6}$
	e_u	$2.643*10^{-4}$	2.007	$6.576*10^{-5}$	2.002	$1.642*10^{-5}$

Table 2: Streamfunction formulation: Compact scheme for $\psi = e^{-t}(x^2+y^2)^2$ with RHS $f = -16e^{-t}(x^2+y^2+4)$ on $[0,1]\times[0,1]$ - l_2 error, relative l_2 error and max error in the horizontal component of velocity field.

We turn now to the class of driven cavity problems, which has been used for benchmark test problems by many authors. In particular, we compare our results to the steady state results of Ghia, Ghia and Shin [10]. First we show numerical results for $\nu = 1/400$. Here the domain is $\Omega = [0,1]\times[0,1]$ and the fluid is driven in the $x-$direction on the top section of the boundary ($y=1$). Thus, $u=1,\ v=0$ for $y=1$, and $u=v=0$ for $x=0,\ x=1$ and $y=0$. In Table 3 we present computational quantities for different meshes and time-levels. We show $\psi^{\Omega,t} = \max_{\Omega}\psi(x,y,t)$, $(\bar{x},\bar{y})$, where $(\bar{x},\bar{y})$ is the point where $\psi^{\Omega,t}$ occurs, and $\psi_{\Omega,t} = \min_{\Omega}\psi(x,y,t)$. The meshes are of $65\times 65,\ 81\times 81$ and 97×97 points and the time levels are $t = 10, 20, 40, 60$. Note that the highest value of the streamfunction at the latest time step is 0.1136. Here the maximum occurs at $(\bar{x},\bar{y}) = (0.5521, 0.6042)$, and the minimal value of the streamfunction is $-6.498*10^{-4}$. Note that $\psi^{\Omega,t}$ in Table 3 has been stabilized at $t=40$. The location $(\bar{x},\bar{y})$ of the primary vortex remains constant from $t=20$ and on. In [10] $\psi^{\Omega,t} = 0.1139$ occurs at $(0.5547, 0.6055)$, and the minimal value of the streamfunction is $-6.424*10^{-4}$. Figure 2a displays streamfunction contours at $t=60$, using a 97×97 mesh. In Figure 4a we present velocity components $u(0.5,y)$ and $v(x,0.5)$ (solid lines) at $T=60$ compared with values obtained in [10] (marked by '0'), for $\nu = 1/400$. Note that the match between the results is excellent.

time	quantity	65×65	81×81	97×97
10	$\max \psi$	0.1053	0.1057	0.1059
	$(\bar{x}, \bar{y})$	$(0.5781, 0.6250)$	$(0.5750, 0.6250)$	$(0.5833, 0.6354)$
	$\min \psi$	$-4.786 * 10^{-4}$	$-4.758 * 10^{-4}$	$-4.749 * 10^{-4}$
20	$\max \psi$	0.1124	0.1128	0.1130
	$(\bar{x}, \bar{y})$	$(0.5625, 0.6094)$	$(0.5625, 0.6125)$	$(0.5521, 0.6042)$
	$\min \psi$	$-6.333 * 10^{-4}$	$-6.371 * 10^{-4}$	$-6.361 * 10^{-4}$
40	$\max \psi$	0.1131	0.1134	0.1136
	$(\bar{x}, \bar{y})$	$(0.5625, 0.6094)$	$(0.5500, 0.6000)$	$(0.5521, 0.6042)$
	$\min \psi$	$-6.513 * 10^{-4}$	$-6.5148 * 10^{-4}$	$-6.498 * 10^{-4}$
60	$\max \psi$	0.1131	0.01134	0.1136
	$(\bar{x}, \bar{y})$	$(0.5625, 0.6094)$	$(0.5500, 0.6000)$	$(0.5521, 0.6042)$
	$\min \psi$	$-6.514 * 10^{-4}$	$-6.5155 * 10^{-4}$	$-6.498 * 10^{-4}$

Table 3: Streamfunction Formulation: Compact scheme for the driven cavity problem, $Re = 400$. [10]'s results: $\max \psi = 0.1139$ at $(0.5547, 0.6055)$, $\min \psi = -6.424 * 10^{-4}$.

In Table 4 we show the same flow quantities as in Table 3, but for $\nu = 1/1000$ at $t = 20, 40, 60, 80$. The grids are of 65×65, 81×81 and 97×97 points. Note that with each of the meshes the flow quantities tend to converge to a steady state as time progresses. At the latest time level on the finest grid the maximal value of ψ is 0.1178, compared to 0.1179 in [10]. The maximum is obtained at $(\bar{x}, \bar{y}) = (0.5312, 0.5625)$, compared to $(0.5313, 0.5625)$ in [10]. The minimum value of the streamfunction is -0.0017, same as in [10]. Figure 2b displays streamfunction contours at $t = 80$, using a 97×97 mesh. In Figure 4b we present velocity components $u(0.5, y)$ and $v(x, 0.5)$ (solid lines) at $T = 80$ compared with values obtained in [10] (marked by '0'), for $\nu = 1/1000$. Note again the excellent match between the results.

time	quantity	65×65	81×81	97×97
20	$\max \psi$	0.1129	0.1139	0.1143
	$(\bar{x}, \bar{y})$	$(0.5469, 0.5781)$	$(0.5375, 0.5750)$	$(0.5417, 0.5729)$
	$\min \psi$	-0.0015	-0.0015	-0.0015
40	$\max \psi$	0.1160	0.1169	0.1175
	$(\bar{x}, \bar{y})$	$(0.5312, 0.5625)$	$(0.5250, 0.5625)$	$(0.5312, 0.5625)$
	$\min \psi$	-0.0017	-0.0017	-0.0017
60	$\max \psi$	0.1160	0.1171	0.1177
	$(\bar{x}, \bar{y})$	$(0.5312, 0.5625)$	$(0.5250, 0.5625)$	$(0.5312, 0.5625)$
	$\min \psi$	-0.0017	-0.0017	-0.0017
80	$\max \psi$	0.1160	0.1172	0.1178
	$(\bar{x}, \bar{y})$	$(0.5312, 0.5625)$	$(0.5250, 0.5625)$	$(0.5312, 0.5625)$
	$\min \psi$	-0.0017	-0.0017	-0.0017

Table 4: Streamfunction Formulation: Compact scheme for the driven cavity problem, $Re = 1000$ [10]'s results: $\max \psi = 0.1179$ at $(0.5313, 0.5625)$, $\min \psi = -0.0017$.

Results for $\nu = 1/3200$ on a 81×81 mesh and a 97×97 mesh are shown in Table 5. At the latest time level on the finest grid the maximal value of ψ is 0.1174, compared

to 0.1204 in [10]. The latter is obtained at $(\bar{x}, \bar{y}) = (0.5208, 0.5417)$, compared to $(0.5165, 0.5469)$ in [10]. The minimum value of the streamfunction is -0.0027, where [10] reports on -0.0031. Figure 3a displays streamfunction contours at $t = 360$, using a 97×97 mesh. In Figure 5a we present velocity components $u(0.5, y)$ and $v(x, 0.5)$ (solid lines) at $T = 360$ compared with values obtained in [10] (marked by '0'), for $\nu = 1/3200$. There is an excellent match.

time	quantity	81×81	97×97
40	$\max \psi$	0.1157	0.1145
	$(\bar{x}, \bar{y})$	$(0.5125, 0.5500)$	$(0.5104, 0.5417)$
	$\min \psi$	-0.0024	-0.0025
80	$\max \psi$	0.1152	0.1154
	$(\bar{x}, \bar{y})$	$(0.5125, 0.5375)$	$(0.5208, 0.5417)$
	$\min \psi$	-0.0026	-0.0027
160	$\max \psi$	0.1155	0.1169
	$(\bar{x}, \bar{y})$	$(0.5125, 0.5375)$	$(0.5208, 0.5417)$
	$\min \psi$	-0.0026	-0.0027
200	$\max \psi$	0.1155	0.1172
	$(\bar{x}, \bar{y})$	$(0.5125, 0.5375)$	$(0.5208, 0.5417)$
	$\min \psi$	-0.0027	-0.0027
240	$\max \psi$	0.1156	0.1173
	$(\bar{x}, \bar{y})$	$(0.5125, 0.5375)$	$(0.5208, 0.5417)$
	$\min \psi$	-0.0027	-0.0027
360	$\max \psi$	0.1156	0.1174
	$(\bar{x}, \bar{y})$	$(0.5125, 0.5375)$	$(0.5208, 0.5417)$
	$\min \psi$	-0.0027	-0.0027

Table 5: Streamfunction Formulation: Compact scheme for the driven cavity problem, $Re = 3200$ [10]'s results: $\max \psi = 0.1204$ at $(0.5165, 0.5469)$, $\min \psi = -0.0031$.

Finally, in Table 6 we display results for $\nu = 1/5000$. At the latest time level on the finest grid the maximal value of ψ is 0.1160, compared to 0.11897 in [10]. The location of the maximal value is $(\bar{x}, \bar{y}) = (0.5104, 0.5417)$, compared to $(0.5117, 0.5352)$ in [10]. The minimum value of the streamfunction is -0.0029, where the value -0.0031 was found in [10]. Figure 3b displays streamfunction contours at $t = 400$, with a 97×97 mesh. In Figure 5b we present velocity components $u(0.5, y)$ and $v(x, 0.5)$ (solid lines) at $T = 400$ compared with values obtained in [10] (marked by '0'), for $\nu = 1/5000$. Note the excellent match in this case too.

time	quantity	81×81	97×97
40	$\max \psi$	0.0936	0.0983
	$(\bar{x}, \bar{y})$	$(0.4875, 0.6125)$	$(0.5114, 0.6146)$
	$\min \psi$	-0.0029	-0.0030
80	$\max \psi$	0.1007	0.1010
	$(\bar{x}, \bar{y})$	$(0.5000, 0.5125)$	$(0.5312, 0.5312)$
	$\min \psi$	-0.0027	-0.0029
120	$\max \psi$	0.1060	0.1068
	$(\bar{x}, \bar{y})$	$(0.5125, 0.5375)$	$(0.5104, 0.5417)$
	$\min \psi$	-0.0028	-0.0028
160	$\max \psi$	0.1095	0.1105
	$(\bar{x}, \bar{y})$	$(0.5125, 0.5375)$	$(0.5104, 0.5312)$
	$\min \psi$	-0.0028	-0.0028
200	$\max \psi$	0.1117	0.1127
	$(\bar{x}, \bar{y})$	$(0.5125, 0.5375)$	$(0.5104, 0.5312)$
	$\min \psi$	-0.0028	-0.0029
240	$\max \psi$	0.1131	0.1141
	$(\bar{x}, \bar{y})$	$(0.5125, 0.5375)$	$(0.5104, 0.5417)$
	$\min \psi$	-0.0028	-0.0029
280	$\max \psi$	0.1139	0.1150
	$(\bar{x}, \bar{y})$	$(0.5125, 0.5375)$	$(0.5104, 0.5417)$
	$\min \psi$	-0.0028	-0.0029
400	$\max \psi$	0.1149	0.1160
	$(\bar{x}, \bar{y})$	$(0.5125, 0.5375)$	$(0.5104, 0.5417)$
	$\min \psi$	-0.0028	-0.0029

Table 6: Streamfunction Formulation: Compact scheme for the driven cavity problem, $Re = 5000$ [10]'s results: $\max \psi = 0.11897$ at $(0.5117, 0.5352)$, $\min \psi = -0.0031$.

We also investigated the behavior of the flow for $\nu = 1/7500$ and $\nu = 1/10000$. Here, the initial flow was taken from the results of $\nu = 1/5000$ at $T = 400$. For $\nu = 1/7500$ at $T = 560$ with a 97×97 mesh, the maximal value of ψ is 0.1175, compared to 0.11997 in [10]. The location of the maximal value is $(\bar{x}, \bar{y}) = (0.5104, 0.5312)$, compared to $(0.5117, 0.5322)$ in [10]. The minimum value of the streamfunction is -0.003, where the value -0.0033 was found in [10]. Figure 6a displays streamfunction contours and Figure 7a represents velocity components $u(0.5, y)$ and $v(x, 0.5)$ (solid lines) compared with values obtained in [10] (marked by '0'). The match is excellent.

For $\nu = 1/10000$ at $T = 500$ with a 97×97 mesh, the maximal value of ψ is 0.1190, compared to 0.1197 in [10]. The location of the maximal value is $(\bar{x}, \bar{y}) = (0.5104, 0.5312)$, compared to $(0.5117, 0.5333)$ in [10]. The minimum value of the streamfunction is -0.0033, where the value -0.0034 was found in [10]. Figure 6b displays streamfunction contours and Figure 7b represents velocity components $u(0.5, y)$ and $v(x, 0.5)$ (solid lines) compared with values obtained in [10] (marked by '0'). Note again that the match between the computed $u(0.5, y)$ and $v(x, 0.5)$ at $T = 500$ and [10]'s results is excellent. However, a steady state has not been reached, as we can observe from Figure 8b, which represents the maximal value of the streamfunction from

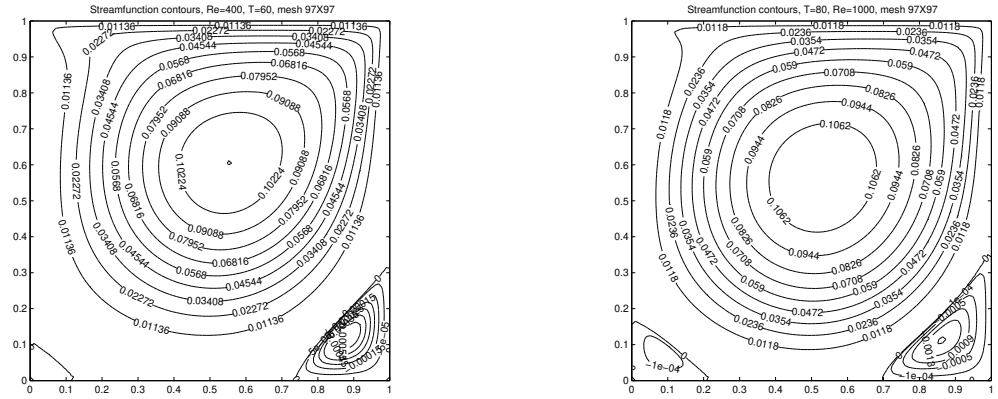

(a) Re=400 (b) Re=1000

Figure 2: Driven Cavity for $Re = 400, 1000$: Streamfunction Contours

T=400 to $T = 500, \nu = 1/10000$. A similar plot- Figure 8a- shows that for $\nu = 1/7500$ the same quantity grows monotonically toward a steady-state, while for $\nu = 1/10000$ we observe that it grows non-monotonically. A similar phenomena was observed for $\nu = 1/8500$, in agreement with [17] and [12]. Therefore, it seems that in [10] a steady state solution was computed, however the solution of the time-dependent problem does not tend to a steady state. A similar phenomenon was observed in [17], [12], [19]. It is commonly interpreted as an indication that, while a steady state solution is computed in [10] for high Reynolds numbers, they are unstable and experience a Hopf bifurcation into time-periodic solutions. The rigorous analysis proving this bifurcation has not yet been performed.

A similar problem, that we considered, has the same geometry Ω, but here the fluid is driven also in the negative $y-$direction at the left-end of Ω. Thus, $u = 1,\ v = 0$ for $y = 1,\ u = 0,\ v = -1$ for $x = 0,\ u = v = 0$ for $x = 1$ and $y = 0$. We picked $\nu = 1/400, 1/1000, 1/3200, 1/5000$ and started the flow impulsively from zero. Figures 9a-9b and 10a-10b represent the streamfunction at $t = 100$ for the various viscosity coefficients, respectively. Note that at $\nu = 1/3200$ we start to observe symmetry breaking with 81×81 and 97×97 meshes. Numerical results by Pan and Glowinski [17] indicate the same phenomena for $1/\nu$ between 4000 and 5000. In Figures 11a-b the maximum of the streamfunction from $T = 0$ to $T = 200$ is displayed, for $Re = 3200$ and $Re = 5000$, respectively. A closer look to $T = 400$ shows that no steady state is achieved for both cases. Figures 12a-b shows the same quantities as in Figures 11a-b, for for $T = 200$ to $T = 400$

Acknowledgements. Supported in part by funds from the Israel Science Foundation (ST).

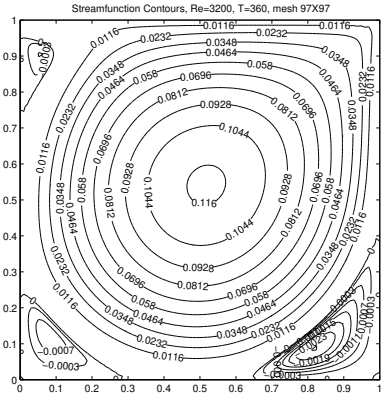

(a) Re=3200

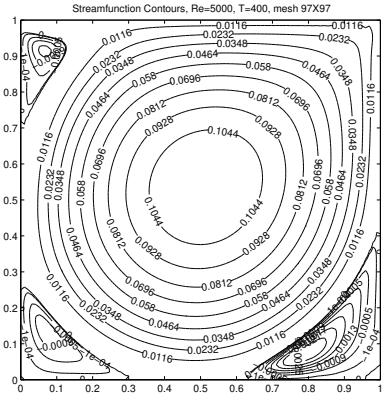

(b) Re=5000

Figure 3: Driven Cavity for $Re = 3200, 5000$: Streamfunction Contours

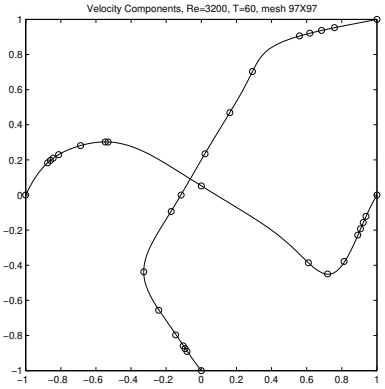

(a) Re=400

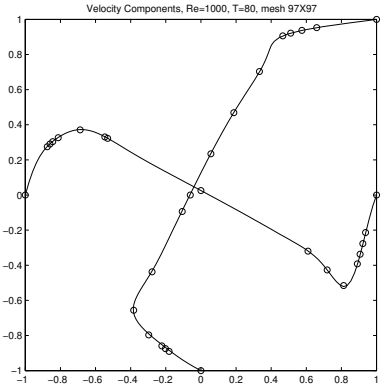

(b) Re=1000

Figure 4: Driven Cavity for $Re = 400, 1000$: Velocity Components. [10]'s results are marked by '0'

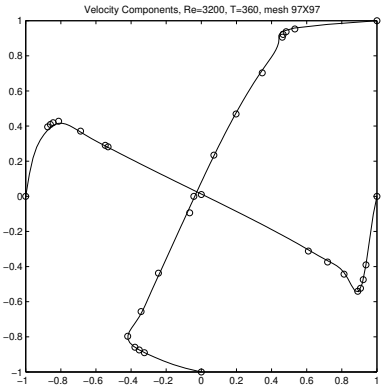

(a) Re=3200

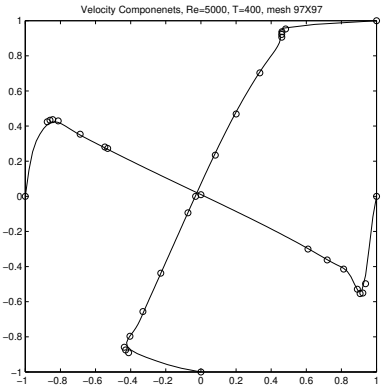

(b) Re=5000

Figure 5: Driven Cavity for $Re = 3200, 5000$: Velocity Components. [10]'s results are marked by '0'

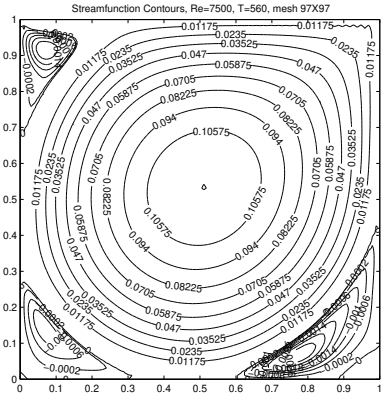

(a) Re=7500

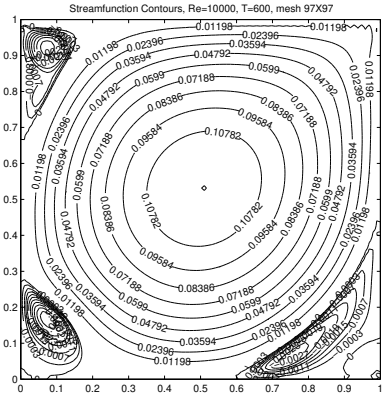

(b) Re=10000

Figure 6: Driven Cavity for $Re = 7500, 10000$: Streamfunction Contours, (a): max $\psi = 0.1175$, [10]'s 0.11998; location is $(0.5104, 0.5312)$, [10]'s $(0.5117, 0.5322)$; min$\psi = -0.0030$, [10]'s $= -0.0033$. (b): max $\psi = 0.1190$, [10]'s 0.1197; location is $(0.5104, 0.5312)$, [10]'s $(0.5117, 0.5333)$; min$\psi = -0.0033$, [10]'s $= -0.0034$.

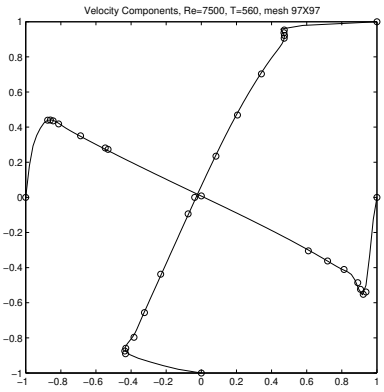

(a) Re=7500

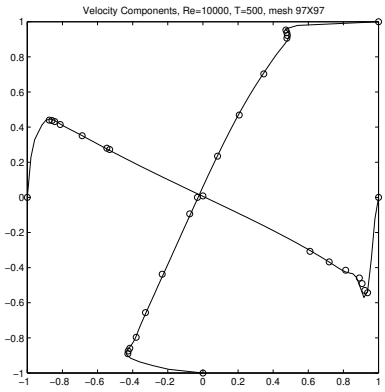

(b) Re=10000

Figure 7: Driven Cavity for $Re = 7500, 10000$: Velocity Components. [10]'s results are marked by '0'

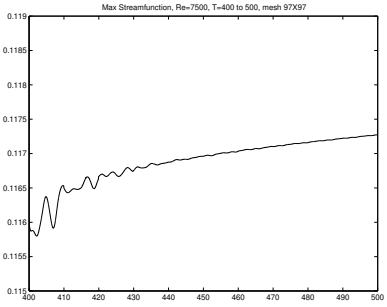

(a) Re=7500

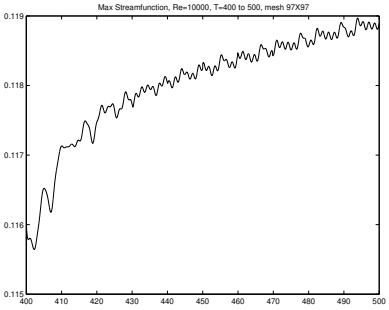

(b) Re=10000

Figure 8: Driven Cavity for $Re = 7500, 10000$: Max Streamfunction, T=400 to 500.

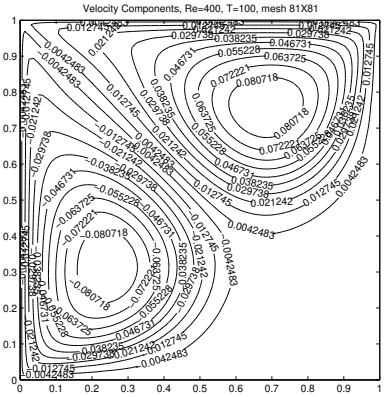

(a) Re=400

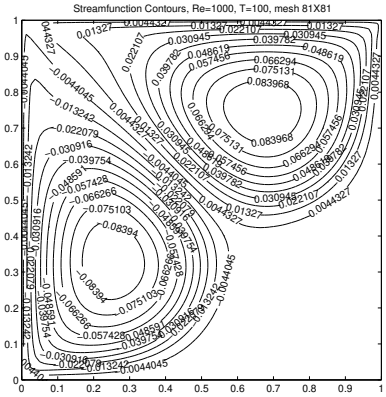

(b) Re=1000

Figure 9: Double Driven Cavity for $Re = 400, 1000$: Streamfunction Contours

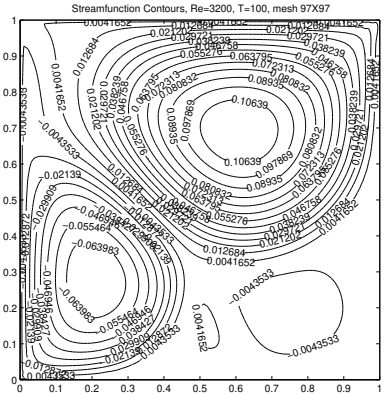

(a) Re=3200

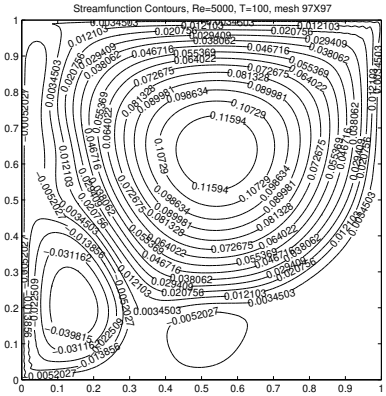

(b) Re=5000

Figure 10: Double Driven Cavity for $Re = 3200, 5000$: Streamfunction Contours

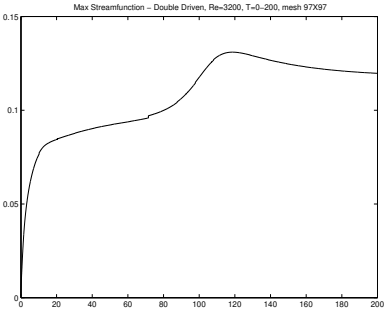

(a) Re=3200

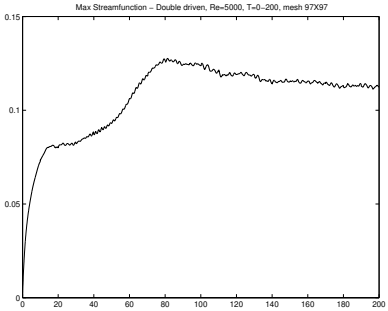

(b) Re=5000

Figure 11: Double Driven Cavity for $Re = 3200, 5000$: Max Streamfunction, T=0 to 200.

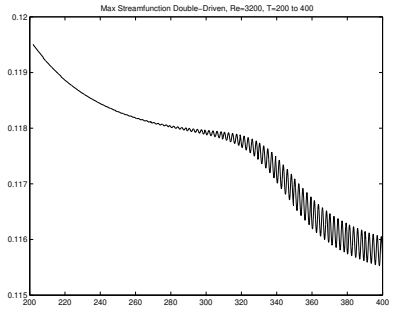

(a) Re=3200

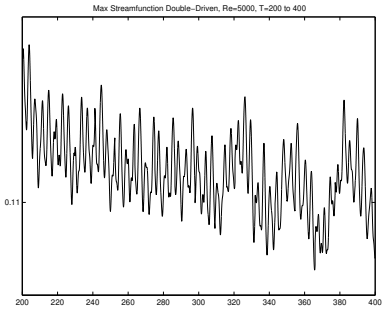

(b) Re=5000

Figure 12: Double Driven Cavity for $Re = 3200, 5000$: Max Streamfunction, T=200 to 400.

References

[1] I. Altas, J. Dym, M. M. Gupta, and R. P Manohar. Mutigrid solution of automatically generated high-order discretizations for the biharmonic equation. *SIAM J.Sci.Comput.*, 19:1575–1585, 1998.

[2] M. Ben-Artzi. Vorticity dynamics in planar domains. in preparation.

[3] M. Ben-Artzi, D. Fishelov, and S. Trachtenberg. Vorticity Dynamics and Numerical Resolution of Navier-Stokes Equations. *Math. Model. Numer. Anal.*, 35(2):313–330, 2001.

[4] D. Calhoun. A cartesian grid method for solving the two-dimensional streamfunction-vorticity equations in irregular regions. *J.Comp.Phys.*, 176:231–275, 2002.

[5] A. J. Chorin. Numerical solution of the Navier-Stokes equations. *Math.Comp.*, 22:745–762, 1968.

[6] G.-H. Cottet and P.D. Koumoutsakos. *Vortex Methods. Theory and Practice.* Cambridge Univ. Press, 2000.

[7] W. E and J.-G. Liu. Essentially compact schemes for unsteady viscous incompressible flows. *J. Comp.Phys.*, 126:122–138, 1996.

[8] W. E and J.-G. Liu. Vorticity boundary condition and related issues for finite difference scheme. *J. Comp.Phys.*, 124:368–382, 1996.

[9] D. Fishelov, M. Ben-Artzi, and J.-P. Croisille. A compact scheme for the streamfunction formulation of navier-stokes equations. *Notes on Computer Science (Springer Verlag)*, 2667:809–817, 2003.

[10] U. Ghia, K. N. Ghia, and C. T. Shin. High-Re solutions for incompressible flow using the Navier-Stokes equations and a multigrid method. *J. Comp. Phys.*, 48:387–411, 1982.

[11] P. M. Gresho. Incompressible fluid dynamics: some fundamental formulation issues. *Annu. Rev. Fluid Mech.*, 23:413–453, 1991.

[12] R. Kupferman. A central-difference scheme for a pure streamfunction formulation of incompressible viscous flow. *SIAM J. Sci.Comput.*, 23, No. 1:1–18, 2001.

[13] H. Lamb. *Hydrodynamics*. Dover, 6-th edition, 1932.

[14] Ming Li and Tao Tang. A compact fourth-order finite difference scheme for unsteady viscous incompressible flows. *J. Sci. Comput.*, 16, No. 1:29–45, 2001.

[15] Zhilin Li and Cheng Wang. A fast finite difference method for solving navier-stokes equations in irregular domains. *Comm. Math. Sci.*, 1, No. 1:180–196, 2003.

[16] J. L. Lions and E. Magenes. *Non-Homogeneous Boundary Value Problems and Applications I*. Springer-Verlag, 1972.

[17] T. W. Pan and R. Glowinski. A projection/wave-like equation method for the numerical simulation of incompressible viscous fluid flow modeled by the Navier-Stokes equations. *Comput. Fluid Dynamics*, 9, 2000.

[18] L. Quartapelle. *Numerical Solution of the Incompressible Navier-Stokes Equations*. Birkhauser Verlag, 1993.

[19] J. Shen. Hopf bifurcation of the unsteady regularized driven cavity. *J.Comp.Phys.*, 95:228–245, 1991.

[20] J. W. Stephenson. Single cell discretizations of order two and four for biharmonic problems. *J.Comp.Phys.*, 55:65–80, 1984.

[21] R. Temam. *Navier-Stokes Equations*. AMS Edition, 2001.

[22] T. E. Tezduyar, J. Liou, D. K. Ganjoo, and M. Behr. Solution techniques for the vorticity-streamfunction formulation of the two-dimensional unsteady incompressible flows. *Int. J. for Num. Meth. in Fluids*, 11:515–539, 1990.